

Satellite galaxies in the Illustris-1 simulation: anisotropic locations around relatively isolated hosts

Tereasa G. Brainerd[★] and Masaya Yamamoto

Boston University, Department of Astronomy, 725 Commonwealth Ave., Boston, MA, USA 02215

Accepted XXX. Received YYY; in original form ZZZ

ABSTRACT

We investigate the locations of luminous satellite galaxies in the $z = 0$ redshift slice of the hydrodynamical Illustris-1 simulation. As expected from previous studies, the satellites are distributed anisotropically in the plane of the sky, with a preference for being located near the major axes of their hosts. Due to misalignment of mass and light within the hosts, the degree of anisotropy is considerably less when the mean satellite location is measured with respect to the hosts' stellar surface mass density than when it is measured with respect to the hosts' dark matter surface mass density. When measured with respect to the hosts' dark matter surface mass density, the mean satellite location depends strongly on host stellar mass and luminosity, with the satellites of the faintest, least massive hosts showing the greatest anisotropy. This is caused by a strong correlation between the degree of anisotropy in the plane of the sky and host-satellite proximity in 3-d. The satellites of the faintest, least massive hosts are dominated by objects that are close to their hosts in 3-d, whereas the satellites of the brightest, most massive hosts are dominated by objects that are far from their hosts in 3-d. When measured with respect to the hosts' stellar surface mass density, the mean satellite location is essentially independent of host stellar mass and luminosity. The satellite locations are, however, dependent upon the stellar masses of the satellites, with the most massive satellites having the most anisotropic distributions.

Key words: galaxies: dwarf – galaxies: haloes – dark matter

1 INTRODUCTION

Small, faint satellite galaxies, in orbit around large, bright ‘host’ galaxies, have the potential to yield information about the relationship between dark and luminous matter within the host galaxies. In particular, the spatial distribution of satellite galaxies may yield constraints on the shapes of the hosts' dark matter haloes and on the orientations of the hosts within those haloes. Studies of host-satellite samples selected from large redshift surveys such as the Two Degree Field Galaxy Redshift Survey (2dFGRS; Colless et al. 2001, 2003) and the Sloan Digital Sky Survey (SDSS; Fukugita et al. 1996; Hogg et al. 2001; Smith et al. 2002; Strauss et al. 2002; York et al. 2000) have shown that, in the case of relatively isolated host galaxies, the satellites exhibit a spatial anisotropy with respect to the luminous major axes of their hosts. When averaged over all satellites and all hosts, the satellites of relatively isolated host galaxies are found preferentially close to the hosts' major axes (Sales & Lambas 2004, 2009; Brainerd 2005; Azzaro et al. 2007; Bailin et

al. 2008; Ágústsson & Brainerd 2010, 2011). The degree to which observed satellite galaxies exhibit a spatial anisotropy has also been shown to be strongly dependent upon the physical properties of the hosts and satellites (Sales & Lambas 2004, 2009; Azzaro et al. 2007; Bailin et al. 2008; Ágústsson & Brainerd 2010, 2011). In host-satellite samples obtained from large redshift surveys of the observed universe, the most pronounced tendency for satellites to be found near their hosts' major axes occurs for hosts that have high stellar masses, low star formation rates and are red in colour. Further, satellites that have high stellar masses, low star formation rates and are red in colour show a much greater spatial anisotropy than do satellites that have low stellar masses, high star formation rates and are blue in colour.

Since Cold Dark Matter (CDM) haloes are triaxial (e.g., Jing & Suto 2002), an anisotropy in the satellite locations is expected if satellites are fair tracers of their hosts' dark matter haloes and if, in projection on the sky, the luminous host galaxies are well-aligned with the halo mass density. Ágústsson & Brainerd (2006; hereafter AB06) investigated the locations of satellite galaxies in the $z = 0$ redshift slice of the Λ CDM GIF simulation (Kauffmann et al. 1999), which com-

[★] E-mail: brainerd@bu.edu (TGB)

bined a semi-analytic galaxy formation model (‘SAM’) with an adaptive particle-particle-particle-mesh N-body simulation. AB06 found that, if mass and light were perfectly aligned within the hosts, the degree of anisotropy in the satellite locations was similar to that of the halo dark matter, with the mean satellite location measured with respect to the luminous hosts’ major axes, $\langle\phi_{\text{sat}}\rangle$, being only slightly less than the mean location of the dark matter particles, $\langle\phi_{\text{dm}}\rangle$. When AB06 allowed the degree of alignment between mass and light in the host galaxies to vary, the resulting locations of the satellites, again measured with respect to the luminous hosts’ major axes, varied from being nearly isotropic (caused by aligning the angular momenta of the luminous hosts with the net angular momenta of the hosts’ dark matter haloes) to a complete reversal of the expected distribution, with the satellites showing a preference for being located near the hosts’ *minor* axes (caused by aligning the angular momenta of the luminous hosts with the largest principle axes of the hosts’ dark matter haloes).

Ágústsson & Brainerd (2010; hereafter AB10) investigated the locations of the satellites of relatively isolated host galaxies in a mock redshift survey of the first Millennium simulation (MS; Springel et al. 2005). The luminous galaxies in AB10 were obtained from the DeLucia & Blaizot (2007) SAM, which included rest-frame luminosities in multiple bandpasses and *B*-band bulge-to-disc ratios. AB10 embedded the luminous host galaxies within their dark matter haloes in various ways, and they explored the effects of different host galaxy orientations on the resulting satellite locations. Using the *B*-band bulge-to-disc ratio, AB10 divided their hosts into those with expected disc morphologies and those with expected elliptical morphologies. AB10 found that the only way they could reproduce the observed dependence of SDSS satellite locations on host colour, stellar mass, and star formation rate was for the MS host galaxies to be embedded within their dark matter haloes in markedly different ways: mass and light had to be well-aligned in elliptical hosts, resulting from a model in which luminous ellipticals were essentially miniature versions of their dark matter haloes, and mass and light had to be poorly-aligned within disc hosts, resulting from a model in which the angular momenta of the luminous discs were aligned with the net angular momenta of their dark matter haloes. Within a given host morphological class (i.e., elliptical vs. disc), AB10 found that the locations of the MS satellites were *independent* of the hosts’ stellar mass and star formation rate, and it was only by combining the locations of the satellites of both elliptical and disc MS hosts that the observed dependence of SDSS satellite locations on host colour, stellar mass and star formation rate could be reproduced by the MS.

More recently, Dong et al. (2014; hereafter Dong14) explored the locations of satellite galaxies in a Λ CDM simulation that included smoothed-particle hydrodynamics. Unlike AB10, who had the liberty of choosing the ways in which the luminous hosts were oriented within their dark matter haloes, Dong14 were restricted to the use of the luminous, stellar particles to define the orientations of their hosts. Dong14 used the stellar particles to compute reduced inertia tensors, the eigenvalues of which were used to define the hosts’ luminous major and minor axes in the plane of the sky. Dong14 concluded that, on average, satellite galaxies were found preferentially close to the major axes of their

luminous hosts, with the degree of satellite anisotropy being most pronounced for satellites with the highest metallicities. Over all, Dong14 found that the mean satellite location, measured with respect to the hosts’ luminous major axes, was essentially independent of satellite stellar mass and was weakly-dependent on both the host stellar mass and the host halo virial mass, with the satellites of the most massive hosts showing the greatest degree of anisotropy. Dong14 do not discuss the details of the host and satellite selection criteria for their sample, so it is unclear whether their systems are directly comparable to those in AB10. The minimum satellite stellar mass in Dong14 is an roughly an order of magnitude larger than the minimum satellite stellar mass in AB10; however, the range of host stellar masses in Dong14 is similar to that of AB10.

In the case of relatively isolated hosts, studies of the 3-d locations of satellite galaxies obtained from SAMs are generally in agreement that the satellites trace the underlying dark matter mass distribution (see, e.g., Sales et al. 2007; Wang et al. 2014). However, Ágústsson & Brainerd (2018) found that the degree to which MS satellites traced the underlying mass distributions of their hosts was a strong function of the physical properties of the hosts, with the satellites of red hosts tracing the 3-d host mass distribution well and the satellites of blue hosts having a 3-d spatial distribution that was twice as concentrated as the hosts’ dark matter mass. In addition, a study of the 3-d spatial distributions of satellite galaxies in the hydrodynamical Illustris-1 simulation by Brainerd (2018) showed that the satellites do not trace the hosts’ mass distributions at all well on scales less than 50% of the halo virial radius. If it is the case that satellite galaxies do not, in general, trace their hosts’ mass distributions, then the interpretation of any observed spatial anisotropy becomes particularly complicated.

In this paper we use the high-resolution hydrodynamical Illustris-1 simulation to obtain a sample of relatively isolated host galaxies and their satellites, and we further explore the locations of satellites with respect to their hosts. Illustris-1 is the highest resolution simulation produced by the original Illustris Project (Vogelsberger et al. 2014a; Nelson et al. 2015). At the present epoch (i.e., $z = 0$), the gravitational force softening length in Illustris-1 is 710 pc, the smallest hydrodynamical gas cells are 48 pc in extent and the simulation contains $\sim 40,000$ resolved, luminous galaxies. The simulation volume is a cubical box with comoving sidelength of $L = 106.5$ Mpc. Periodic boundary conditions, 1820^3 dark matter particles of mass $m_p = 6.3 \times 10^6 M_\odot$, and 1820^3 hydro cells with an initial baryonic mass resolution of $1.3 \times 10^6 M_\odot$ were used. Compared to the simulation used by Dong14, the mass resolution of Illustris-1 is ~ 100 times greater and the force resolution is ~ 6 times greater, allowing significantly better resolution of both the luminous host galaxies and their satellites. The values of the cosmological parameters adopted for the Illustris Project are: $\Omega_m = 0.2726$, $\Omega_\Lambda = 0.7274$, $\Omega_b = 0.0456$, $\sigma_8 = 0.809$, $n_s = 0.963$, and $H_0 = 70.4 \text{ km s}^{-1} \text{ Mpc}^{-1}$. All data used for our analysis are publicly available through the Illustris Project website: <http://www.illustris-project.org>.

The paper is organized as follows. In §2 we discuss the selection criteria for our host-satellite sample and we summarise various sample properties. In §3 we use the full sample of hosts and satellites to compute the locations of the

satellites, in projection on the sky, with respect to the major axes of the hosts' dark matter mass and the hosts' stellar mass. In §3 we also discuss the dependence of the locations of the satellites as a function of various physical properties of the hosts and satellites, as well as host-satellite separation. In §4 we compute the locations of the satellites from a subsample of the full host-satellite sample, where the properties of the subsample are similar to those of the host-satellite sample in AB10. In §5 we present a summary and discussion of our major results.

2 HOST-SATELLITE SAMPLE

Observational studies of the locations of satellite galaxies have often adopted selection criteria that were intended to yield a sample of large, bright host galaxies that are relatively isolated from similarly large, bright galaxies. These relatively isolated host galaxies are surrounded by a sample of smaller, fainter satellite galaxies that are located within a distance of ~ 500 kpc of their hosts (see, e.g., Sales & Lambas 2004, 2009; Brainerd 2005; Azzaro et al. 2007; Bailin et al. 2008; AB10; Ágústsson & Brainerd 2011). In the observed universe, host-satellite samples are always contaminated to some degree by ‘interlopers’ (i.e., false satellites whose locations on the sky, apparent magnitudes and line of sight velocities relative to a particular host place them within the satellite sample but they are, in fact, located too far from the host to be genuine satellites). In a simulation we have full phase space information for all galaxies and, unlike observational studies that must rely on redshift space selection, here we adopt selection criteria in real space that incorporate the 3-d distances between the host galaxies and their satellites. That is, in our analysis of the locations of Illustris-1 satellites we focus only on those objects which might be considered to be genuine satellites and our sample does not include the interlopers that are inevitably found in observational catalogs.

In order to select hosts that are relatively isolated from similarly large, bright galaxies, all hosts were required to be at least 2.5 times brighter than any other galaxy found within a radius of 700 kpc. In addition, because we wish to focus on host galaxies that are sufficiently massive that they would have ‘regular’ morphologies in the observed universe, hosts were required to have stellar masses range $10^{10} M_{\odot} \leq M_{*}^{\text{host}} \leq 10^{12} M_{\odot}$. Lastly, all host galaxies were required to be located at the centres of their friends-of-friends haloes. This final requirement insured that the hosts were located at the centres of the potential wells within which the satellites were moving. Satellite galaxies were then defined to be all other galaxies with absolute magnitudes $M_r < -14.5$ (i.e., comparable to the resolution limit for luminous galaxies at $z = 0$; see, e.g., the $z = 0$ Illustris-1 galaxy luminosity function in Vogelsberger et al. 2014b), located within a radius of 500 kpc of the host.

Applying the above criteria to the $z = 0$ timestep of Illustris-1 resulted 2,341 host galaxies with a total of 10,928 satellites. The median host virial mass is $M_{200} = 10^{12} M_{\odot}$ and the median host virial radius is $r_{200} = 205$ kpc. The median host and satellite absolute magnitudes are $M_r^{\text{host}} = -21.8$ and $M_r^{\text{sat}} = -16.6$, the median host and satellite stellar masses are $\log_{10}(M_{*}^{\text{host}}/M_{\odot}) = 10.5$ and $\log_{10}(M_{*}^{\text{sat}}/M_{\odot}) = 7.1$, and the

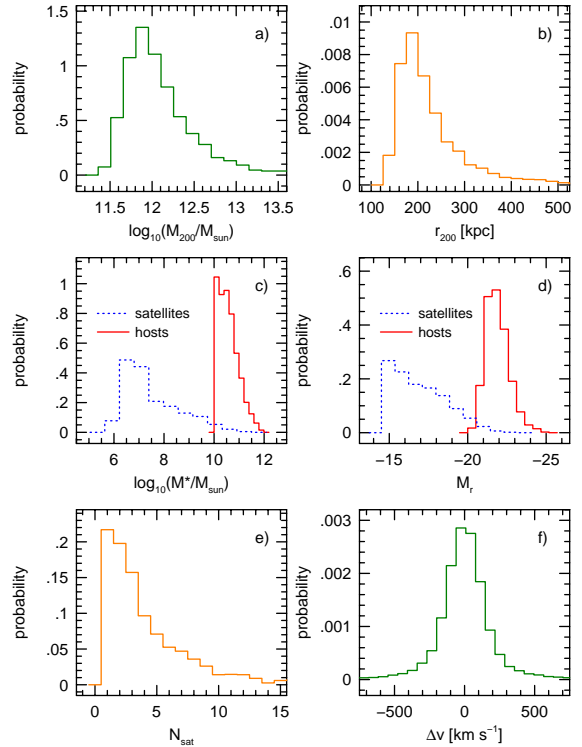


Figure 1. Normalized probability distributions for various properties of the host-satellite sample: a) host virial mass, b) host virial radius, c) host and satellite stellar masses, d) host and satellite absolute magnitudes, e) number of satellites per host, and f) line of sight velocity differences between the hosts and satellites.

median number of satellites per host is $N_{\text{sat}} = 3$. Figure 1 shows normalized probability distributions for various properties of the host-satellite sample. Compared to the host-satellite sample in AB10, our sample contains hosts with similar luminosities, stellar masses and halo virial masses. Our satellite sample extends to fainter luminosities and smaller stellar masses than does AB10’s sample, however, and, because we did not impose a maximum line of sight velocity difference between our hosts and satellites, the distribution of host-satellite velocity differences extends somewhat beyond the value of $|dv|_{\text{max}} = 500$ km/s imposed by AB10.

3 SATELLITE LOCATIONS: COMPLETE SAMPLE

In analogy with observational studies, for which the satellite locations are determined in the plane of the sky, here we compute the locations of the Illustris-1 satellites as viewed along each of the three principle axes of the simulation box. Throughout, we show results for the satellite locations computed as an average over these three independent projections. For a particular host-satellite pair, the satellite location, ϕ , is given by the angle between the major axis of the surface mass density of the host and the direction vector that connects the centroids of the host and satellite, as viewed in projection along a particular axis. Since we are primarily interested in whether the satellites show a preference for being

aligned with either the major or minor axes of their hosts, we restrict ϕ to the range $[0^\circ, 90^\circ]$, where $\phi = 0^\circ$ indicates alignment with the host major axis, $\phi = 90^\circ$ indicates alignment with the host minor axis, and a mean satellite location of $\langle \phi \rangle = 45^\circ$, computed over many host-satellite pairs, indicates a distribution that is isotropic on average.

We define each host’s dark matter distribution to be the distribution of the dark matter particles within the host’s virial radius (i.e., the Illustris Project ‘Group_M_Crit200’ data field). Further, we define each host’s stellar mass distribution to be the distribution of the stellar particles contained within the radius at which the host’s surface brightness profile drops below $20.7 \text{ mag arcsec}^{-2}$ in *K*-band (i.e., the Illustris Project ‘SubhaloStellarPhotometricsRad’ data field). The host galaxies are well resolved, allowing accurate determinations of the relative orientations of their dark and luminous components. The number of dark matter particles in the hosts’ dark matter haloes ranges from 2.0×10^3 to 3.3×10^7 and the number of stellar particles contained within the host galaxies themselves ranges from 7.0×10^3 to 1.1×10^6 . We use the hosts’ dark matter and stellar particles to compute mass weighted moments of the dark matter and stellar surface mass densities as $I_{xx} \equiv \sum_{i=1}^N m_i x_i^2$, $I_{yy} \equiv \sum_{i=1}^N m_i y_i^2$, $I_{xy} \equiv \sum_{i=1}^N m_i x_i y_i$, and we define the host ellipticity to be $\epsilon = 1 - b/a$ where a and b are, respectively, the semi-major and semi-minor axis lengths.

3.1 Locations Averaged over all Satellites

We begin our investigation by computing the mean satellite location using all host-satellite pairs. For each host-satellite pair, we compute ϕ separately for two different definitions of the host surface mass density: [1] the dark matter mass of the host’s halo (i.e., the dark matter mass contained within the halo virial radius) and [2] the stellar mass of the luminous host galaxy. Averaged over the entire sample of hosts and satellites, the mean satellite location is $\langle \phi \rangle = 38.1^\circ \pm 0.1^\circ$ when ϕ is computed using the major axes of the hosts’ dark matter haloes and $\langle \phi \rangle = 42.8^\circ \pm 0.1^\circ$ when $\langle \phi \rangle$ is computed using the major axes of the hosts’ stellar mass. That is, as expected from previous studies, when the locations of the satellites are averaged over the entire sample, the satellites have a preference for being located near the major axes of their hosts, and the anisotropy is considerably more pronounced when ϕ is measured with respect to the major axes of the hosts’ dark matter haloes than when it is measured with respect to the hosts’ luminous mass.

The reduction in the satellite spatial anisotropy that occurs when ϕ is computed using the hosts’ stellar mass distribution is due to the fact that the hosts’ stellar mass distribution is not perfectly aligned with the hosts’ dark matter mass distribution. Figure 2 shows the mean offset between the position angle of the hosts’ stellar mass distribution, θ_{star} , and the position angle of the hosts’ dark matter mass distribution, θ_{dm} , as a function of host *r*-band absolute magnitude (top panel), host stellar mass (middle panel), and ellipticity (bottom panel). From the top and middle panels of Figure 2, the mean offset between the hosts’ dark matter surface mass density and stellar surface mass density is substantial, and is essentially independent of host stellar mass and absolute magnitude. This results in a significant

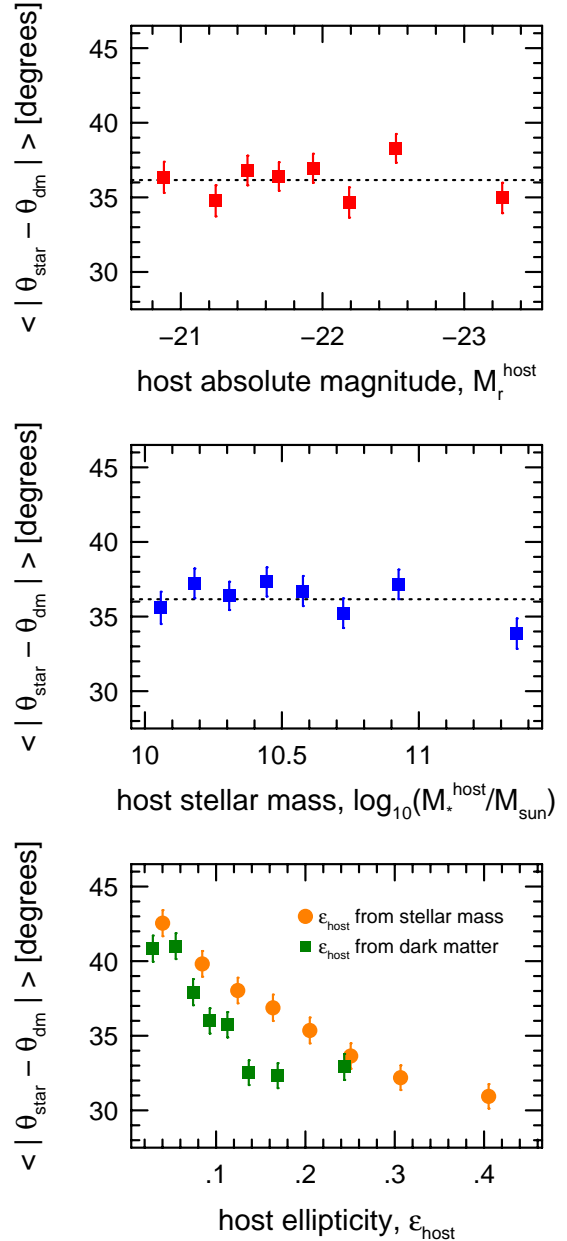


Figure 2. Mean offset between the hosts’ stellar surface mass distribution and dark matter surface mass distribution, $\langle |\theta_{\text{star}} - \theta_{\text{dm}}| \rangle$. *Top:* Dependence of $\langle |\theta_{\text{star}} - \theta_{\text{dm}}| \rangle$ on host absolute magnitude. *Middle:* Dependence of $\langle |\theta_{\text{star}} - \theta_{\text{dm}}| \rangle$ on host stellar mass. *Bottom:* Dependence of $\langle |\theta_{\text{star}} - \theta_{\text{dm}}| \rangle$ on host ellipticity, for two different measures of the ellipticity: stellar particles (orange circles) and dark matter particles (green squares).

reduction in the degree of anisotropy in the satellite locations when they are measured relative to the hosts’ stellar mass distribution. The bottom panel of Figure 2 shows that the degree of offset between the hosts’ stellar surface mass density and dark matter surface mass density is a strong function of host ellipticity, independent of whether the host ellipticity is defined to be that of stellar mass or the dark matter halo. That is, the bottom panel of Figure 2 shows the mean offset between the hosts’ stellar mass and dark

matter distributions is greatest for the roundest hosts, but it is significant even in the case of the flattest hosts. Note that the data in Figure 2 are binned such that there are a nearly identical number of objects per bin, resulting in similarly-sized error bars for each bin.

3.2 Dependence of Locations on Host Properties

Here we compute the mean locations of the satellites as a function of various host properties. In order to assess the degree to which the satellites trace the host mass distribution in projection on the sky, we first compute $\langle\phi\rangle$ for the satellites and for the mass particles as a function of host ellipticity. The top panel of Figure 3 shows the mean satellite location, $\langle\phi_{\text{sat}}\rangle$, and the mean dark matter particle location, $\langle\phi_{\text{dm}}\rangle$, as a function of the ellipticity of the hosts' haloes. In the top panel of Figure 3, ϕ is computed relative to the major axes of the hosts' dark matter surface mass density. The bottom panel of Figure 3 shows the mean satellite location, $\langle\phi_{\text{sat}}\rangle$, and the mass weighted mean stellar particle location, $\langle\phi_{\text{star}}\rangle$, as a function of the ellipticity of the hosts' stellar mass distribution. In the bottom panel of Figure 3, ϕ is computed relative to the major axes of the hosts' stellar surface mass density. From top panel of Figure 3, then, the satellite distribution is significantly flatter (i.e., considerably more anisotropic) than is the dark matter distribution surrounding the host galaxies. This result differs from the results of AB06 who found that, in projection on the sky, the satellite distribution was only slightly more anisotropic than the dark matter surrounding the hosts (see the top panel of Figure 3 in AB06). The bottom panel of Figure 3 shows that for all but the very roundest hosts ($\epsilon_{\text{star}} < 0.06$), the satellite distribution is systematically rounder than is the hosts' luminous surface mass density.

Figure 4 shows the dependence of the satellite locations on the projected radius between the hosts and satellites, r_p (top panel), host absolute magnitude, M_r^{host} (middle panel), and host stellar mass, M_*^{host} (bottom panel). Circles indicate that ϕ was computed using the major axes of the hosts' dark matter haloes; diamonds indicate that ϕ was computed using the major axes of the hosts' stellar mass distribution. The data in Figure 4 have been binned such that there are nearly identical numbers of host-satellite pairs in each bin.

From Figure 4, there are significant differences between $\langle\phi\rangle$ when measured relative to the hosts' dark matter surface mass density vs. the hosts' stellar surface mass density. When computed relative to the hosts' stellar mass, $\langle\phi(r_p)\rangle$ indicates that the satellites are distributed nearly isotropically for $r_p \gtrsim 50$ kpc, while on scales $r_p \lesssim 50$ kpc the anisotropy is much more pronounced than when $\langle\phi(r_p)\rangle$ is measured relative to the major axes of the hosts' dark matter haloes. When $\langle\phi(r_p)\rangle$ is computed relative to the major axes of the hosts' dark matter haloes, the degree of anisotropy increases with r_p for projected radii less than 150 kpc, while for $r_p > 150$ kpc the degree of anisotropy decreases with r_p . Over all scales, however, the sense of the satellite anisotropy remains the same: a preference for location near the major axes of the hosts, independent of whether the major axis is that of the dark matter mass or the stellar mass. The results for $\langle\phi(r_p)\rangle$ in the top panel of Figure 4 are in generally good agreement with the results from AB10, who found

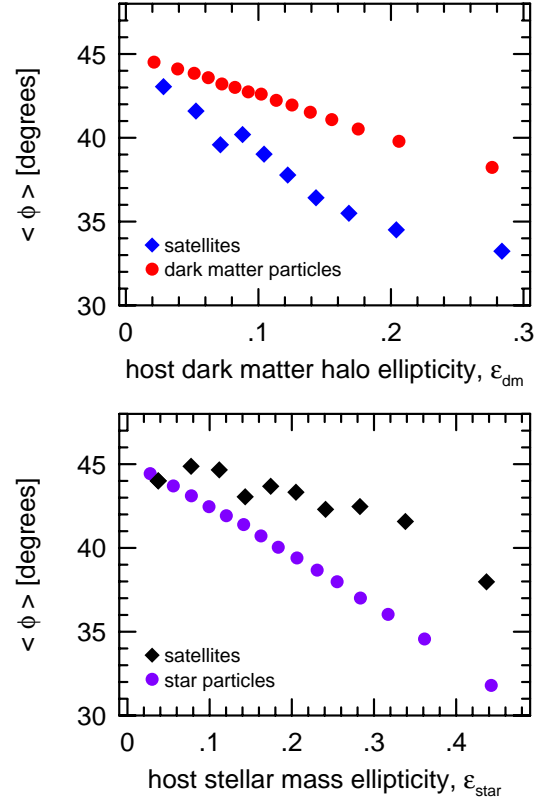


Figure 3. Mean satellite location (diamonds) and mass-weighted mean particle location (circles) as a function of host ellipticity. *Top:* Location of satellites and dark matter particles measured with respect to the major axes of the hosts' dark matter surface mass densities; ellipticity is that of the hosts' dark matter haloes. *Bottom:* Location of satellites and stellar particles, measured with respect to the major axes of the hosts' stellar surface mass densities; ellipticity is that of the hosts' stellar mass. Error bars are omitted since they are comparable to or smaller than the data points.

that, when measured relative to the luminous major axes of the hosts, $\langle\phi(r_p)\rangle$ was only weakly dependent on r_p . For $r_p < 50$ kpc, AB10 found very few satellites in the MS and, because of this, it is not possible to compare our present results for $\langle\phi(r_p)\rangle$ on scales less than 50 kpc to those of AB10.

Also from Figure 4, there are significant differences between the dependence of the satellite locations on host absolute magnitude and stellar mass when $\langle\phi\rangle$ is measured relative to the hosts' dark matter mass vs. the hosts' stellar mass. When measured relative to the major axes of the hosts' stellar mass, $\langle\phi(M_r^{\text{host}})\rangle$ and $\langle\phi(M_*^{\text{host}})\rangle$ are essentially independent of the physical properties of the hosts. In contrast, when $\langle\phi(M_r^{\text{host}})\rangle$ and $\langle\phi(M_*^{\text{host}})\rangle$ are measured with respect to the major axes of the hosts' dark matter haloes, both are monotonically increasing functions. That is, the greater is M_r^{host} or M_*^{host} , the more isotropic is the satellite distribution.

Our results for $\langle\phi(M_*^{\text{host}})\rangle$ in Figure 4 differ from the results of AB10 and Dong14. When measured relative to the hosts' luminous major axes, both AB10 and Dong14 found $\langle\phi(M_*^{\text{host}})\rangle$ to be a monotonically decreasing function

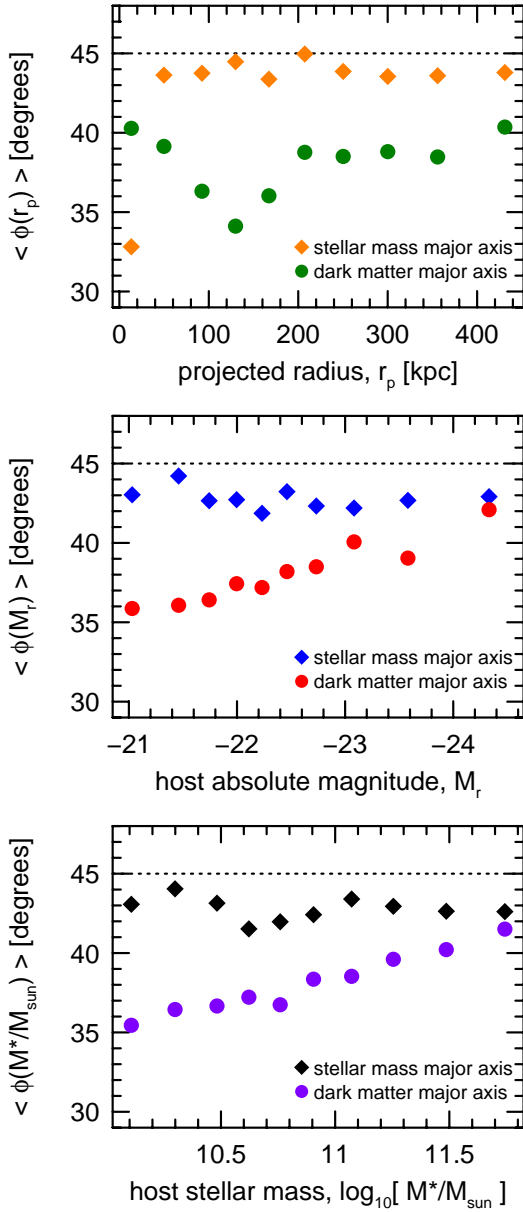


Figure 4. Mean satellite location measured with respect to the hosts’ dark matter major axes (circles) and stellar mass major axes (diamonds). *Top:* Mean satellite location as a function of host-satellite projected radius. *Middle:* Mean satellite location as a function of host absolute r -band magnitude. *Bottom:* Mean satellite location as a function of host stellar mass. Error bars are omitted since they are comparable to or smaller than the data points.

of M_*^{host} (i.e., the satellites of the most massive hosts exhibited a greater degree of anisotropy in their locations than did the satellites of the least massive hosts). AB10 also found the dependence of the satellite location on M_*^{host} to be considerably stronger than did Dong14. In addition, AB10 found that when the locations of the satellites were measured relative to the hosts’ dark matter major axes, $\langle \phi(M_*^{\text{host}}) \rangle$ was inde-

pendent of M_*^{host} , in contrast to the monotonically increasing function that we find in the bottom panel of Figure 4.

3.3 Dependence of Locations on 3-d Host-Satellite Distance

To address differences between previous results and our own for the dependence of the mean satellite location on host stellar mass and absolute magnitude, we compute $\langle \phi \rangle$ as a function of 3-d distances between the hosts and satellites. We also compute the dependence of the radial distribution of satellites on host stellar mass and absolute magnitude. The results are shown in Figure 5. The top panel of Figure 5 shows that when the mean satellite location is computed with respect to the hosts’ dark matter major axes, $\langle \phi \rangle$ is a strong function of the 3-d distance between the hosts and satellites. For satellites located within a distance $r_{3d} \lesssim 180$ kpc, the mean satellite location decreases as a function of r_{3d} , indicating that, on average, the degree of anisotropy in the satellite locations increases with r_{3d} when $r_{3d} \lesssim 180$ kpc. For satellites with 3-d distances $r \gtrsim 200$ kpc (i.e., a distance comparable to the median host virial radius), the mean satellite location increases as a function of r_{3d} , indicating that, on average, the degree of anisotropy in the satellite locations decreases when $r_{3d} \gtrsim 200$ kpc. This is unsurprising since the spatial distribution of satellites that are located outside their hosts’ virial radii should not reflect the shapes of the hosts’ dark matter haloes as well as those that are found within the virial radii.

The middle panel of Figure 5 shows probability distributions for the host-satellite 3-d distances for the most massive 25% of the hosts ($\log_{10}(M^*/M_{\odot}) > 10.81$; red diamonds) and the least massive the 25% of the hosts ($\log_{10}(M^*/M_{\odot}) < 10.24$; blue circles). Vertical lines in the middle panel of Figure 5 indicate the mean virial radii of the two host samples. From the middle panel of Figure 5, in the case of the lowest mass hosts, the number of satellites at a given 3-d host-satellite distance decreases out to distances of $r_{3d} \sim 300$ kpc (i.e., larger than the mean virial radius), beyond which it remains constant. In the case of the the highest mass hosts, the number of satellites at a given 3-d host-satellite distance increases continuously for $r_{3d} \gtrsim 75$ kpc. Because of this, the satellite sample for the lowest mass hosts is dominated by satellites that are close to their hosts, while the satellite sample for the highest mass hosts is dominated by satellites that are far from their hosts.

Since, from the top panel of Figure 5, the mean satellite location is a strong function of r_{3d} , with satellites at $r_{3d} \lesssim 180$ kpc showing a greater degree of anisotropy on average than satellites at $r_{3d} \gtrsim 200$ kpc, the dependence of $\langle \phi(M_{\text{host}}^*/M_{\odot}) \rangle$ in the bottom panel of Figure 4 is a reflection of the 3-d distribution of the satellites. That is, when measured relative to the dark matter major axes of the hosts, the satellites of the least massive hosts show a greater degree of anisotropy in their spatial distribution than do the satellites of the most massive hosts (i.e., purple circles in the bottom panel of Figure 4). This is due to the fact that the satellite population of the low-mass hosts is dominated by nearby satellites, with a high degree of anisotropy in their spatial distribution, while the satellite population for the high mass

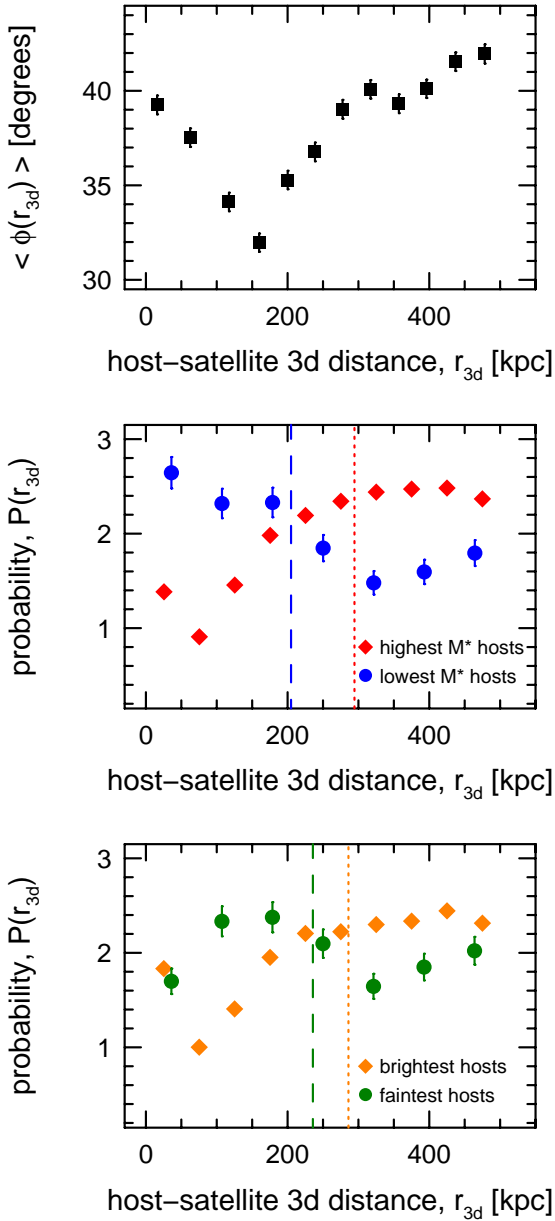


Figure 5. *Top:* Mean satellite location, measured with respect to the hosts’ dark matter major axes, as a function of 3-d host-satellite separation, r_{3d} . *Middle:* Probability distribution for 3-d host-satellite distances as a function of r_{3d} for hosts with $\log_{10}(M^*/M_{\odot}) < 10.24$ (least massive 25% of the hosts; blue circles) and $\log_{10}(M^*/M_{\odot}) > 10.81$ (most massive 25% of the hosts; red diamonds). Vertical lines indicate the mean virial radii of the hosts in the two subsamples (blue dashed line: least massive hosts; red dotted line: most massive hosts). *Bottom:* Probability distribution for 3-d host-satellite distances as a function of r_{3d} for hosts with r -band absolute magnitudes $M_r > -21.36$ (faintest 25% of the hosts; green circles) and $M_r < -22.34$ (brightest 25% of the hosts; orange diamonds). Vertical lines indicate the mean virial radii of the hosts in the two subsamples (green dashed line: least luminous hosts; orange dotted line: most luminous hosts). Error bars are omitted when they are comparable to or smaller than the data points.

hosts is dominated by distant satellites, with a low degree of anisotropy in their spatial distribution.

The bottom panel of Figure 5 shows probability distributions for the host-satellite 3-d distances for the most luminous 25% of the hosts and the least luminous 25% of the hosts. Since stellar mass and luminosity are strongly correlated, the trends for the number of satellites as a function of r_{3d} in the bottom panel of Figure 5 are similar to those in the middle panel of Figure 5, albeit somewhat weaker. Overall, the bottom panel of Figure 5 indicates that the satellite populations of the faintest hosts are dominated by nearby satellites, and the satellite populations of the brightest hosts are dominated by distant satellites. Therefore, the dependence of $\langle \phi(M_r^{\text{host}}) \rangle$ in the middle panel of Figure 4 is also a reflection of the fact that the satellite population for low-luminosity hosts is dominated by nearby satellites, while the satellite population for high-luminosity hosts is dominated by distant satellites.

3.4 Dependence of Locations on Satellite Properties

Figure 6 shows the dependence of the satellite locations on the stellar masses and absolute magnitudes of the satellite galaxies (bottom and top panels, respectively). As expected from the misalignment of dark and luminous mass in the host galaxies, the degree of satellite anisotropy is significantly less when the satellite locations are computed relative to the major axes of the hosts’ stellar mass than when they are computed relative to major axes of the hosts’ dark matter mass. In all cases, $\langle \phi \rangle$ decreases with increasing satellite stellar mass and luminosity. That is, the most massive, most luminous satellites show a greater degree of anisotropy in their locations than do the least massive, least luminous satellites. Dong14 found that, when $\langle \phi \rangle$ was measured relative to the hosts’ stellar mass, the satellite distribution showed no dependence on satellite stellar mass. The satellites in Dong14 were, however, considerably more massive than the majority of our satellites. If we consider only those satellites in a similar stellar mass range, $10^9 M_{\odot} \lesssim M_{\text{sat}}^{\text{sat}} \lesssim 10^{10} M_{\odot}$, our results agree with those of Dong14; the locations of the satellites in this stellar mass range show no dependence on stellar mass. In contrast to our results and those of Dong14, AB10 found that, when measured with respect to the luminous major axes of their hosts, the locations of MS satellites with stellar masses $10^8 M_{\odot} \lesssim M_{\text{sat}}^{\text{sat}} \lesssim 10^{11} M_{\odot}$ showed a strong dependence on $M_{\text{sat}}^{\text{sat}}$, with the most massive satellites being distributed much more anisotropically than the least massive satellites.

4 RESTRICTED HOST-SATELLITE SAMPLE

Our complete sample of hosts and satellites was selected from real space and incorporated 3-d distance information (see §2). In their study, AB10 selected host-satellite systems from a mock redshift survey of the MS in order to better compare the results for MS satellites to the observed locations of satellite galaxies in the SDSS. That is, AB10 selected their host and satellites from the MS using redshift space criteria, rather than selecting them from real space. Because of this, and because our complete sample of satellites contains objects that were too faint to be resolved by the MS, here

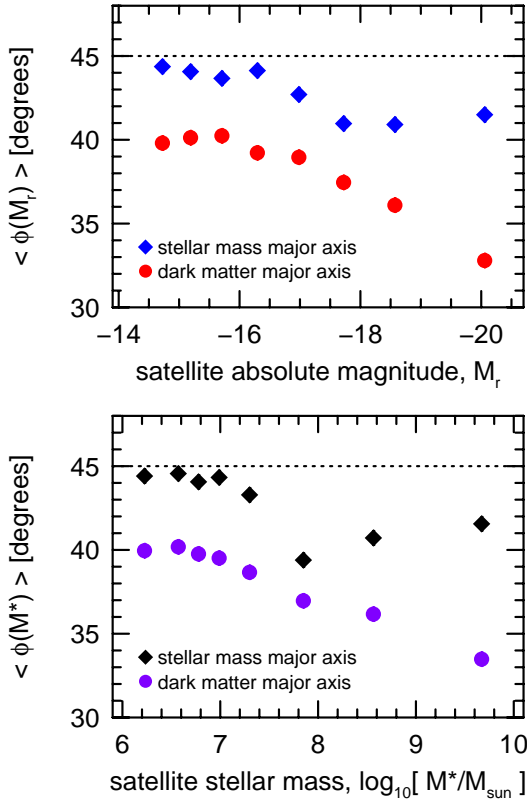


Figure 6. Mean satellite location measured with respect to the hosts’ dark matter major axes (circles) and stellar mass major axes (diamonds). *Top:* Mean satellite location as a function of satellite absolute r -band magnitude. *Bottom:* Mean satellite location as a function of satellite stellar mass. Error bars are omitted since they are comparable to or smaller than the data points.

we investigate the locations of Illustris-1 satellites in a restricted sample that better matches the sample properties of AB10. The properties of the restricted host-satellite sample are the following:

- $-24 \leq M_r^{\text{host}} \leq -20$
- $-22 \leq M_r^{\text{sat}} \leq -17$
- $M_r^{\text{sat}} - M_r^{\text{host}} \geq 2$
- $10^8 M_{\odot} \leq M_{\text{star}}^{\text{sat}} \leq 10^{11} M_{\odot}$
- line of sight relative velocity between a host and its satellites is $|dv| \leq 500 \text{ km s}^{-1}$
- the projected radius between hosts and satellites is $r_p \geq 55 \text{ kpc}$.

The results of measuring $\langle \phi \rangle$ with respect to the hosts’ dark matter and stellar mass for the restricted sample are shown in Figure 7. From Figure 7, the dependence of the mean satellite location on host-satellite projected radius, host absolute magnitude, and host stellar mass in the restricted sample does not differ considerably from the dependence shown by the complete sample in Figure 4. In particular, restricting our host-satellite sample to one with properties similar to that of the sample in AB10 does not resolve the discrepancies between our results for the locations of Illustris-1 satellites and those of AB10 for MS satellites.

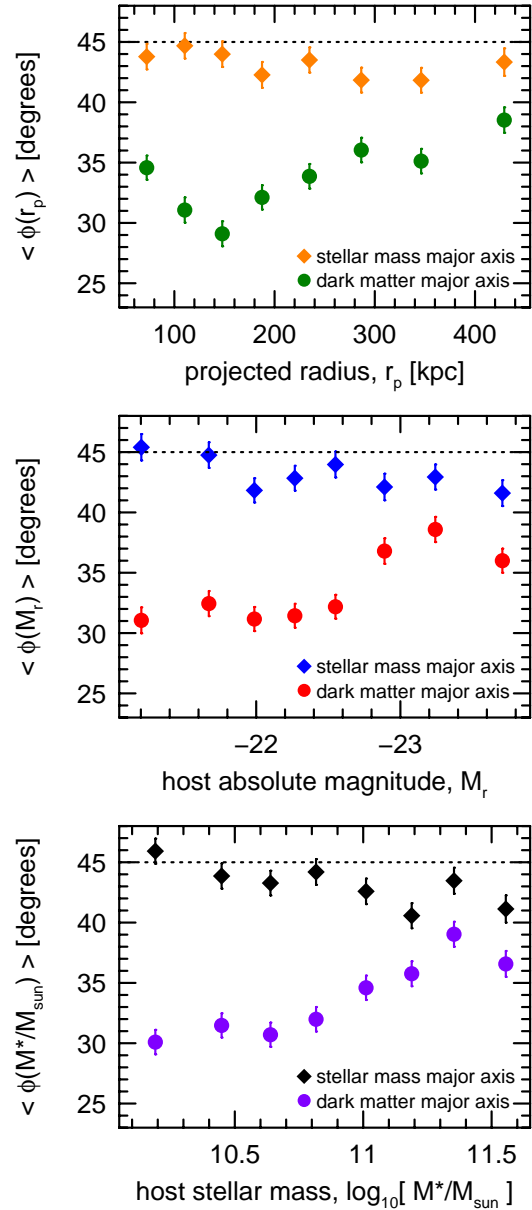


Figure 7. Same as Figure 4 but for the restricted host-satellite sample with properties that better match the MS host-satellite sample in AB10.

5 SUMMARY AND DISCUSSION

We have investigated the locations of luminous satellite galaxies in the hydrodynamical Illustris-1 simulation. The host galaxies were selected to be relatively isolated and the mean satellite location, $\langle \phi \rangle$, was computed separately for two definitions of the host surface mass density: [1] the dark matter mass of the host’s halo and [2] the stellar mass of the luminous host galaxy.

In agreement with previous results, we find that the satellites are distributed anisotropically in the plane of the sky, with a preference for being located near the major axes of their hosts. Due to misalignment between the dark mat-

ter surface mass density and the stellar surface mass density, the degree of anisotropy in the satellite distribution is significantly less when the mean satellite location is measured with respect to the hosts' stellar surface mass density than when it is measured with respect to the hosts' dark matter surface mass density. The mean misalignment between the host stellar surface mass density and dark matter surface mass density is independent of host absolute magnitude and stellar mass, but is strongly dependent on host ellipticity. Overall, the satellite distribution is flatter in projection on the sky than is the dark matter distribution surrounding the host galaxies. With the exception of the roundest host galaxies, the satellite distribution is rounder in projection on the sky than is the hosts' stellar mass distribution.

When measured with respect to the hosts' stellar surface mass density, the mean satellite location is independent of host absolute magnitude and host stellar mass. This differs from the results of AB10 and Dong14, both of whom found that the satellites of the hosts with the largest stellar masses exhibited the greatest degree of anisotropy. When measured with respect to the hosts' dark matter surface mass density, the mean satellite location depends strongly on host absolute magnitude and host stellar mass, with the satellites of the faintest, least massive hosts showing the *greatest* degree of anisotropy. This differs from the results of AB10, who found that the locations of satellite galaxies in the MS were independent of host stellar mass when the locations of the satellites were measured with respect to the hosts' dark matter major axes. We attribute this decrease in the anisotropy of the Illustris-1 satellite locations with host stellar mass and host luminosity to the fact that, for the brightest, most massive hosts, the satellite sample is dominated by objects that are physically distant from their hosts. In the case of the faintest, least massive hosts, the satellite sample is dominated by objects that are physically close to their hosts. Overall, the locations of satellites that are close to their hosts (e.g., within the virial radius) are much more anisotropic than are the locations of satellites that are far from their hosts.

The locations of the brightest, most massive Illustris-1 satellites are more anisotropic than are the locations of the faintest, least massive Illustris-1 satellites. When measured with respect to the host stellar surface mass density, the locations of Illustris-1 satellites with stellar masses in the range $10^8 M_{\odot} \leq M_{*}^{\text{sat}} \leq 10^{10} M_{\odot}$ are independent of satellite stellar mass, in good agreement with the results of AB10 and Dong14.

The cause of the differences between some of our results and those of AB10 and Dong14 are not entirely clear. Restricting our host-satellite sample to a sample with properties similar to that in AB10 does not resolve the differences between our results and theirs. Importantly, however, AB10 made specific assumptions about the orientations of the luminous hosts within their dark matter haloes since the galaxy catalogs in AB10 were based on the results of a SAM, not a hydrodynamical simulation. Dong14 defined the orientation of the host stellar mass in their hydrodynamical simulation in the same way we have done here, but it is not clear how Dong14 selected their host-satellite systems. In particular, it is not clear whether their host-satellite systems are as isolated as ours. Given the different results for satellite locations found by these studies, it will be inter-

esting in future to compare these results to similar analyses of other high-resolution cosmological simulations, including those that incorporate SAMs and those that incorporate numerical hydrodynamics.

ACKNOWLEDGEMENTS

Insightful conversations with Patrick Koh are gratefully acknowledged. This work was partially supported by Boston University's Undergraduate Research Opportunities Program (UROP).

REFERENCES

- Ágústsson I., Brainerd T. G., 2006, *ApJ*, 650, 550 (AB06)
 Ágústsson I., Brainerd T. G., 2010, *ApJ*, 709, 1321 (AB10)
 Ágústsson I., Brainerd T. G., 2011, *ISRAA*, 2011, 958973
 Ágústsson I., Brainerd T. G., 2018, *ApJ*, 862, 169
 Azzaro M., Patiri S. G., Prada F., Zentner A. R., 2007, *MNRAS*, 376, L43
 Bailin J., Power C., Norberg P., Zaritsky D., Gibson B. K., 2008, *MNRAS*, 390, 1133
 Brainerd T. G., 2005, *ApJ*, 628, L101
 Brainerd T. G., 2018, *ApJ Letters*, in press (arXiv:1810.12914)
 Colless M., et al. 2001, *MNRAS*, 328, 1039
 Colless M., et al. 2003, preprint (arXiv:astro-ph/0306581)
 De Lucia G., Blaizot J., 2007, *MNRAS*, 375, 2
 Dong X. C., Lin W. P., Kang X., Wang Y. O., Dutton A. A., Macciò A. V., *ApJ*, 791, L33 (Dong14)
 Fukugita M., Ichikawa T., Gunn J. E., Doi M., Shimasaku K., Schneider D. P., 1996, *AJ*, 111, 1748
 Hogg D. W., Finkbeiner D. P., Schlegel D. J., Gunn J. E., 2001, *AJ*, 122, 2129
 Jing Y. P., Suto Y., 2002, *ApJ*, 574, 538
 Kauffmann G., Colberg J., Diaferio A., White S. D. M., 1999, *MNRAS*, 303, 188
 Nelson D., et al. 2015, *A&C*, 13, 12
 Sales L., Lambas D. G., 2004, *MNRAS*, 348, 1236
 Sales, L. V., Navarro, J. F., Lambas, D. G., White, S. D. M., Croton, D. J. 2007, *MNRAS*, 382, 1901
 Sales L., Lambas D. G., 2009, *MNRAS*, 395, 1184
 Smith J. A., et al., 2002, *AJ*, 123, 2121
 Springel V., et al., 2005, *Nature*, 435, 629
 Strauss M. A., et al., 2002, *AJ*, 124, 1810
 Vogelsberger M., et al., 2014a, *Nature*, 509, 177
 Vogelsberger M., et al., 2014b, *MNRAS*, 444, 1518
 Wang W., Sales L. V., Henriques B. M. B., White S. D. M., 2014, *MNRAS*, 442, 1363
 York D. G., et al., 2000, *AJ*, 120, 1579

This paper has been typeset from a $\text{\TeX}/\text{\LaTeX}$ file prepared by the author.